9

A SCHEME TO ANALYZE SCATTERING FROM FLAT METALLIC PERIODIC STRUCTURES USING THE CONJUGATE-GRADIENT AND THE FAST FOURIER TRANSFORM METHOD

M. F. Cátedra and R. P. Torres

9.1 Introduction
9.2 Formulation of the Continuous Operator Equation
9.3 Formulation of the Discrete Operator Equation
9.4 Computation of the Convolution Integrals Using FFT
9.5 Computation of the Spectral Series
9.6 Results
a. Current Distributions
b. Convergence Study for the Number of Iterations
c. Reflection Coefficients
9.7 Conclusions
Appendix
Acknowledgements
References

9.1 Introduction

Due to the great interest in Flat Periodic Structures (FPS) for antenna and microwave applications, suitable numerical tools are required to analyze and design such structures. The design is based on extensive use of analysis data for different geometrical configurations. Thus, the computational efficiency in analyzing each geometrical configuration is a critical requirement of the design procedure.

A survey of different techniques for the analysis of FPS can be found in [1]. Only two techniques appear to be useful to analyze FPS

with patches of arbitrary geometry including losses. One of them, [2], is based on the Moment Method (MM) and has the disadvantages inherent to it: the requirements of computer time and memory become prohibitive in many problems. The other technique is based on the Conjugate-Gradient and the Fast Fourier Transform Method, [1,3–5], and is rather more efficient than the MM.

The CG-FFT method is applied to solve problems formulated in terms of operator equations such as

$$LI = Y \tag{1}$$

where L is an integrodifferential operator and I and Y are the unknown and excitation functions, respectively. For the Electric Field Integral Equation the operator L has a convolution nature. The Conjugate Gradient Method (CGM) performs operations like LW or L^aW in each iteration, where W is a known function and L^a is the adjoint operator of L. These computations are carried out efficiently using FFT. A general discussion of the application of the CG-FFT method to finite size problems or periodic infinite size problems can be found in [7].

The discrete Fourier transform (or the FFT for fast computation), is specially well suited for FPS problems. That is because it takes advantage of the discrete nature in the spectral domain of the fields and currents, [1,3–5]. In [3] the EFIE is sampled by expanding the induced currents in terms of rooftop functions [8,9], and testing the fields with the same functions. Nearly all the computations involved in the EFIE convolutions are performed in the spectral domain including the EFIE derivatives. In the spectral domain the number of Floquet's harmonics considered in [3] is limited by the size of the FFT considered ($K^{\max}$ the highest frequency considered is $K_x^{\max} = \pi N_x/T_x$ and $K_y^{\max} = \pi N_y/T_y$, T_x and T_y being the side lengths of the generating cell of the periodic lattice). This limitation in the spectral band is justified from the fact that the resulting Floquet's series in this approach are convergent. As reported in [3] the asymptotic form of Floquet's harmonics follows

$$\frac{1}{m\,(m^2+n^2)^{1/2}}\,|J_x^{mn}| \qquad \text{or} \qquad \frac{1}{n\,(m^2+n^2)^{1/2}}\,|J_y^{mn}| \tag{2}$$

where (m,n) is the harmonic order, and $|J_x^{mn}|$ and $|J_y^{mn}|$ are the spectral amplitudes of the induced current components for this har-

monic. The CG-FFT approach proposed here is in part similar to [1] and [3], but with two main differences:

As first difference the efficient numerical technique of [8,9] to treat mixed-potential EFIE, [10], is incorporated in the present CG-FFT scheme. The technique of [8,9] was also applied in [2] to solve FPS using MM. In [4,5] a CG-FFT scheme using this technique was outlined. The advantage of this scheme is that, as shown in [2], Floquet's harmonics decrease as

$$\frac{1}{mn\,(m^2+n^2)^{1/2}}\,|J_x^{mn}| \qquad \text{or} \qquad \frac{1}{mn\,(m^2+n^2)^{1/2}}\,|J_y^{mn}| \tag{3}$$

Now absolute convergence in Floquet's series can be guaranteed a priori. Although the approach of [4,5] has in the spectral domain the same band limitation with [1] and [3], the convergence rate obtained is better since the magnitudes of Floquet's harmonics decrease faster following (3) than (2).

The second main difference between the present approach and that of [3] is of practical and theoretical importance. In the numerical approach the fields are sampled in the real domain at discrete points and therefore the Fourier Transform of the sampled field is periodic, with a period proportional to the inverse of the sampling interval, [11,12]. In addition the length of this period agrees with the bandwidth of the FFT considered. These facts allow, as it is demonstrated in the paper, to perform the EFIE convolutions without limitations in the spectral band, improving the quality of the results and the convergence rates.

This paper is arranged as follows: In Part 2 the EFIE is formulated. Green's function of this EFIE takes into account the periodic character of the fields and currents. This EFIE is sampled in Part 3 using "rooftop" functions to expand the current and "blade-razor" functions to smooth the fields. The smoothed fields are discretized by considering explicitly a sampling function, [12], (a train of impulse functions). Part 3 ends with expressions for the sampled EFIE where all the integrals required to compute the induced fields are expressed in terms of only one kind of convolution. This convolution is computed efficiently using the FFT as shown in Part 4. The fields have a discrete and periodic nature in both domains (real and spectral). In the spectral domain the fields are obtained from the product of two discrete and periodic functions. One of them is the FFT of the discrete function that forms the coefficients of the expansion of the induced current in

terms of rooftops. The other function is obtained from a series, which terms include values of the Continuous Fourier Transform (CFT) of the Green's function considered. Part 5 deals with three approaches to compute this series. Results of current distributions, convergence rates and reflection coefficients for several FPS are given in Part 6. All these results have been obtained using the Conjugate Gradient algorithm that appears in [13]. The paper ends with an Appendix with complete expressions for the sampled operator.

9.2 Formulation of the Continuous Operator Equation

The first step is the continuous operator equation formulation. Figure 9.1 shows the problem to be solved. A plane wave is incident upon a periodic lattice with a rectangular generating cell of area $T_x T_y$.

The induced current on the metallic patches can be obtained by solving the following operator equation [4],

$$\hat{z} \times \overline{E}^i(\overline{r}) = \hat{z} \times \left\{ K_I \int_{S_p} G^F(\overline{r} - \overline{r}') \overline{J}(\overline{r}')\, ds' - K_C \nabla \int_{S_p} G^F(\overline{r} - \overline{r}') \nabla' \overline{J}(\overline{r}')\, ds' \right\}; \quad \text{for} \quad \overline{r}' \in S_p \tag{4}$$

where $\overline{E}^i$ is the incident field shown in Fig. 9.1, $K_I = j\omega\mu/4\pi$, $K_C = 1/(j\omega\epsilon 4\pi)$,
S_p is the conducting surface of the generating cell and G^F is a Green's function that takes into account Floquet's harmonics.

$$G^F(\overline{r}) = \sum_{m=-\infty}^{\infty} \sum_{n=-\infty}^{\infty} G(\overline{r} - \overline{v}_{mn}) \exp\left(-j\overline{K}^i \cdot \overline{v}_{mn}\right) \tag{5}$$

where

$$G(r) = \exp(-jK_o r)/r \tag{6}$$

$$\overline{v}_{mn} = mT_x\hat{x} + nT_y\hat{y} \tag{7}$$

$$\overline{K}^i = k_{ox}\hat{x} + k_{oy}\hat{y} + k_{oz}\hat{z} \tag{8}$$

$$K_o = \omega\sqrt{\mu\epsilon} \tag{9}$$

where $\overline{K}^i$ is the incident wave vector defined in Fig. 9.1.

Expressing the induced current on the reference cell as

$$\overline{J}(\overline{r}) = \overline{J}^o(\overline{r})\,\phi(\overline{r}) \tag{10}$$

where

$$\phi(\overline{r}) = \exp(-jk_{ox}x - jk_{oy}y) \tag{11}$$

Equation (4) can be put in a more compact form as follows

$$E_x^i = E_{xx}^S + E_{xy}^{SC} \qquad \text{for} \quad \overline{r} \in S_p \tag{12a}$$

$$E_y^i = E_{yx}^{SC} + E_{yy}^S \qquad \text{for} \quad \overline{r} \in S_p \tag{12b}$$

where

$$E_{\alpha\alpha}^S = E_{\alpha\alpha}^{SI} + E_{\alpha\alpha}^{SC} \tag{13}$$

and

$$E_{\alpha\alpha}^{SI} = L_{\alpha\alpha}^I J_\alpha^o \tag{14a}$$

$$E_{\alpha\beta}^{SC} = L_{\alpha\beta}^C J_\beta^o \tag{14b}$$

$$L_{\alpha\alpha}^I = K_I \int_{S_p} G^F(\overline{r} - \overline{r}')\,\phi(\overline{r}')\,ds' \tag{15}$$

$$L_{\alpha\beta}^C = K_C \frac{\partial}{\partial\alpha} \int_{S_p} G^F(\overline{r} - \overline{r}')\,\phi(\overline{r}') \left(\frac{\partial}{\partial\beta} - jk_{o\beta}\right) ds \tag{16}$$

9.3 Formulation of the Discrete Operator Equation

Now the continuous system of equations of (12) will be sampled. So the induced current, $\overline{J}^o$, is expanded in terms of rooftop functions, T_x^{ij} and T_y^{ij} as follows

$$J_\alpha^o(\overline{r}) = \sum_{i=0}^{N_x-1} \sum_{j=0}^{N_y-1} J_\alpha^D(i,j)\,T_\alpha^{ij}(\overline{r}), \qquad \text{for} \quad \alpha = x \text{ or } y \tag{17}$$

where $J_\alpha^D(i,j)$ is a discrete function. Definitions of T_x^{ij} and T_y^{ij} can be found elsewhere, [8,9]. Figure 9.2 shows an example of a rooftop function. Figure 9.3 shows the approximation to the geometry using these basis functions. It should be noticed that the continuous geometry of the plates is approximated by a set of small rectangles of size

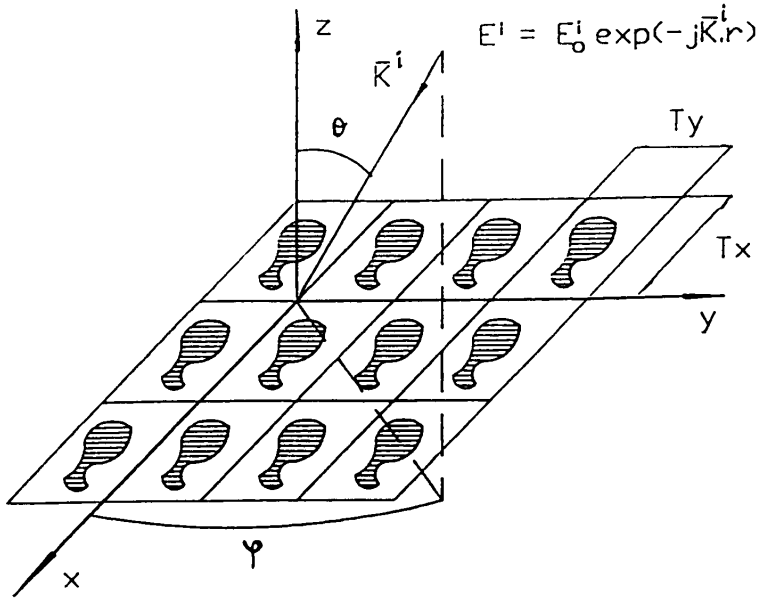

Figure 9.1 Geometry of the Flat Periodic Structure.

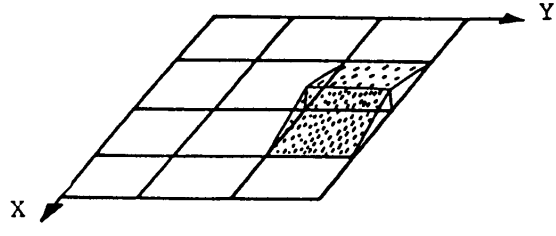

Figure 9.2 Example of rooftop for the x-component of the current.

$\Delta x \Delta y = (T_x/N_x)(T_y/N_y)$. Rooftop functions T_x^{ij} and T_y^{ij} have their centers located at the points

$$\bar{r}_x^{ij} = i\Delta x\hat{x} + (j - 1/2)\Delta y\hat{y}, \qquad \text{for} \quad T_x^{ij} \tag{18a}$$

$$\bar{r}_y^{ij} = (i - 1/2)\Delta x\hat{x} + j\Delta y\hat{y}, \qquad \text{for} \quad T_y^{ij} \tag{18b}$$

The discrete functions $J_x^D(i,j)$ and $J_y^D(i,j)$ must be zero at the point (i,j) such that its corresponding rooftop function is located

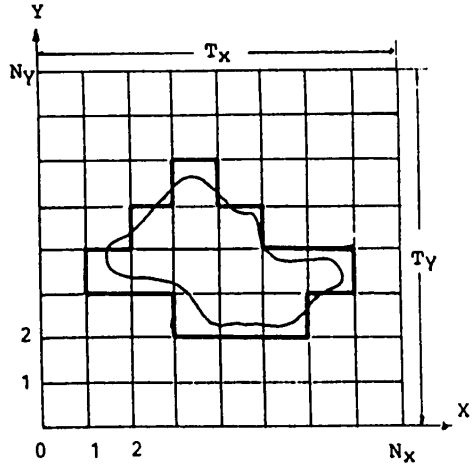

Figure 9.3 The continuous geometry of an arbitrary patch is approximated by a set of small rectangles.

outside the metallic plates. To take this into account we define the geometrical discrete functions $g^x(i,j)$ and $g^y(i,j)$ to be equal to zero when the corresponding rooftop function is located outside the metallic plates and equal to unity otherwise. A more detailed description of these geometrical functions can be found in [13].

For the sake of coherence in the formulation the following functions will be defined

$$J_x^{D\Delta}(i,j) = \left(J_x^D(i,j) + J_x^D(i-1,j)\right) \tag{19a}$$

$$J_y^{D\Delta}(i,j) = \left(J_y^D(i,j) + J_y^D(i,j-1)\right) \tag{19b}$$

$$J_x^{D\delta}(i,j) = \left(J_x^D(i,j) - J_x^D(i-1,j)\right)/\Delta x \tag{20a}$$

$$J_y^{D\delta}(i,j) = \left(J_y^D(i,j) \vdash J_y^D(i,j-1)\right)/\Delta y \tag{20b}$$

where $i = 0,1,2,\ldots,N_x - 1$, and $j = 0,1,2,\ldots,N_y - 1$

All the discrete functions defined here are considered periodic with a reference cell of size (N_x, N_y).

"Blade razor" functions, R_x and R_y have been considered to smooth the fields. These functions are defined as follows

$$R_x(\bar{r}) = \begin{cases} 1, & \text{for } |x| \leq \Delta x/2,\ y = 0 \\ 0, & \text{elsewhere} \end{cases} \tag{21a}$$

$$R_y(\bar{r}) = \begin{cases} 1, & \text{for } |y| \leq \Delta y/2,\ x = 0 \\ 0, & \text{elsewhere} \end{cases} \tag{21b}$$

Discrete functions are obtained from the impressed and scattered fields by first performing a convolution of these fields with R_x or R_y and then by sampling at discrete points the resulting continuous functions. For instance for the impressed fields we have

$$E_\alpha^{iD}(\bar{r}) = III(\bar{r}_\alpha^{mn}) \int_{S_p} E_\alpha^i(\bar{r}')\, R_\alpha(\bar{r} - \bar{r}')\, ds' \tag{22}$$

where $III(\bar{r}_\alpha^{mn})$ indicates the two dimensional sampling function:

$$III(\bar{r}_\alpha^{mn}) = \sum_{m=-\infty}^{\infty} \sum_{n=-\infty}^{\infty} \delta(x - x_\alpha^{mn})\, \delta(y - y_\alpha^{mn}) \tag{23}$$

where δ indicates the impulse function.

Applying (22) to the plane wave excitation indicated in Fig. 9.1 we have

$$E_\alpha^{iD}(\bar{r}) = III(\bar{r}_\alpha^{mn}) \left[\phi(\bar{r})\, \Delta\alpha E_{o\alpha}^i \mathrm{sinc}(K_{o\alpha} \Delta\alpha/2) \right] \tag{24}$$

The sampling procedure proposed in (22) can appear surprising and confusing at first glance, but in fact in [1–5] and in almost all the MM applications, a sampling with $III(r)$ is implicitly made. In (22) authors only write explicitly a quite commonly used sampling procedure.

The following discrete system of equations is obtained from (12) by the sampling process indicated in (22):

$$E_x^{iD}(\bar{r}) = -E_x^{SD}(\bar{r}); \qquad \text{for} \quad g^x(m,n) = 1 \tag{25a}$$

$$E_y^{iD}(\bar{r}) = -E_y^{SD}(\bar{r}); \qquad \text{for} \quad g^y(m,n) = 1 \tag{25b}$$

where

$$E_\alpha^{SD} = E_{\alpha\alpha}^{SD} + E_{\alpha\beta}^{SDC}; \qquad \alpha = x \text{ or } y \tag{26}$$

$$E_{\alpha\alpha}^{SD} = E_{\alpha\alpha}^{SDI} + E_{\alpha\alpha}^{SDC} \tag{27}$$

The terms $E_{\alpha\alpha}^{SDI}$, $E_{\alpha\alpha}^{SDC}$ are developed next. For $E_{\alpha\alpha}^{SDI}$ we have

$$E_{\alpha\alpha}^{SDI}(\bar{r}) = III(\bar{r}_\alpha^{mn}) \int_{S_p} R_\alpha(\bar{r}-\bar{r}') E_{\alpha\alpha}^{SI}(\bar{r}')\, ds'$$
$$\approx III(\bar{r}_\alpha^{mn})\, \Delta\alpha E_{\alpha\alpha}^{SI}(\bar{r}) = III(\bar{r}_\alpha^{mn})\, \Delta\alpha L_{\alpha\alpha}^{I} J_\alpha^o$$
$$\approx III(\bar{r}_\alpha^{mn})\, \Delta\alpha L_{\alpha\alpha}^{I} \sum_{i=0}^{N_s-1} \sum_{j=0}^{N_y-1} J_\alpha^D P_\alpha^{ij}(\bar{r}')\, ds'$$
$$= III(\bar{r}_\alpha^{mn})\, \Delta\alpha \int_{S_p} G^f(\bar{r}-\bar{r}')\, \phi(\bar{r}) \sum_{i=0}^{N_s-1} \sum_{j=0}^{N_y-1} J_\alpha^D P_\alpha^{ij}(\bar{r}')\, ds' \quad (28)$$

where $P_\alpha^{mn}(\bar{r})$ is a two-dimensional pulse defined over a small rectangle of area $\Delta x \Delta y$ centered at $\bar{r}_\alpha^{mn}$. To obtain the last expression in (28) we have assumed that $E_{\alpha\alpha}^{SI}$ is constant for all the points where R_α does not vanish and equal to its value at the center point of R_α. The rooftop T_α^{ij} has been approximated by the pulse P_α^{ij} that has the same volume and center point that T_α^{ij}. These two approximations are justified in [8].

The terms $E_{\alpha\alpha}^{SDC}$ or $E_{\alpha\beta}^{SDC}$ are developed as follows

$$E_{\alpha\beta}^{SDI}(\bar{r}) = III(\bar{r}_\alpha^{mn}) \int_{S_p} R_\alpha E_{\alpha\beta}^{SC}(\bar{r}')\, ds'$$
$$= III(\bar{r}_\alpha^{mn}) \int_{r_\alpha^-}^{r_\alpha^+} \frac{\partial}{\partial\alpha} V(\bar{r})\, \phi(\bar{r})\, d\alpha$$
$$= III(\bar{r}_\alpha^{mn}) \left[V(\bar{r}_\alpha^+)\, \phi(\bar{r}_\alpha^+) - V(\bar{r}_\alpha^-)\, \phi(\bar{r}_\alpha^-)\right]$$
$$\approx III(\bar{r}_\alpha^{mn})\, \phi(\bar{r}) \left[V(\bar{r}_\alpha^+) - V(\bar{r}_\alpha^-) - jK_{o\alpha}\Delta\alpha \frac{V(\bar{r}_\alpha^+) + V(\bar{r}_\alpha^-)}{2}\right] \quad (29)$$

where

$$\bar{r}_\alpha^{\pm} = \bar{r} \pm \frac{\Delta\alpha}{2}\hat{\alpha} \quad (30)$$
$$V(\bar{r}) = \phi^*(\bar{r}) \int_{S_p} G^F(\bar{r}-r')\, \phi(\bar{r}') \left(\frac{\partial}{\partial\beta} - jK_{o\beta}\right) J_\beta^o(\bar{r}')\, ds'$$
$$\approx \frac{\phi^*(\bar{r})}{\Delta\beta} \int_{S_p} G^F(\bar{r}-\bar{r}')\, \phi(\bar{r}') \sum_{m'=0}^{N_s-1} \sum_{n'=0}^{N_y-1} P_{m'n'}^Q$$

$$\left[J_\beta^{D\delta}\left(m',n'\right) - jK_{o\beta}\Delta\beta J_\beta^{D\Delta}\left(m',n'\right)\right] ds' \tag{31}$$

where $P^Q_{m'n'}$ is a two-dimensional pulse function over the small rectangle of area $\Delta x\Delta y$ with center at $\bar{r} = (m'-1/2)\Delta x\hat{x} + (n'-1/2)\Delta y\hat{y}$. ϕ^* represents the complex conjugate of ϕ.

9.4 Computation of the Convolution Integrals Using FFT

All the integrals required to compute the scattered fields of (25) have been written in terms of convolution integrals as indicated in (28) and (29)–(31). These convolutions can be expressed as

$$W^\delta(\bar{r}) = III(\bar{r}^{mn})\, W(\bar{r}) \tag{32}$$

where

$$\bar{r}^{mn} = x^m\hat{x} + y^n\hat{y} = (m-1/2)\Delta x\hat{x} + (n-1/2)\Delta y\hat{y} \tag{33}$$

$$m = 0,1,2,\ldots,N_x-1; \qquad n = 0,1,2,\ldots,N_y-1$$

$$W(\bar{r}) = \int_{S_p} G^F\left(\bar{r}-\bar{r}'\right) S\left(\bar{r}'\right) ds' \tag{34}$$

$$S\left(\bar{r}'\right) = \phi\left(\bar{r}'\right) \sum_{i=0}^{N_x-1}\sum_{j=0}^{N_y-1} S^D(i,j) P^{ij}\left(\bar{r}'\right) \tag{35}$$

In (35) $P^{ij}(\bar{r}')$ is a two-dimensional pulse function of area $\Delta x\Delta y$, centered at $\bar{r}^{ij}$, and $S^D(i,j)$ is a discrete function.

The function $W^\delta(\bar{r})$ can be computed by following the procedure

$$W^\delta(\bar{r}) = \frac{1}{(2\pi)^2} F^{-1}\left\{F\left(III\left(\bar{r}^{mn}\right)\right) \otimes F\left(W\left(\bar{r}\right)\right)\right\} \tag{36}$$

where $F(F^{-1})$ denotes direct (inverse) continuous Fourier transform

$$F(f(x)) = \int_{-\infty}^{\infty} f(x) e^{-jKx} dx \tag{37}$$

and the symbol $\otimes$ indicates convolution.

Using the properties of the sampling function III, [11,12], the convolution of (36) can be computed as

$$\widetilde{W}^{\delta}(\overline{K}) = \frac{1}{\Delta x \Delta y} F\left(III\left(\overline{r}^{mn}\right)\right) \otimes F\left(W\left(\overline{r}\right)\right)$$

$$= \frac{1}{\Delta x \Delta y} \sum_{m'=-\infty}^{\infty} \sum_{n'=-\infty}^{\infty} \widetilde{W}\left(K_x - m' T_x^K, K_y - n' T_y^K\right) \quad (38)$$

where

$$\widetilde{W}(\overline{K}) = F\left(W\left(\overline{r}\right)\right) \quad (39)$$

$$T_\alpha^K = 2\pi/\Delta\alpha; \qquad \alpha = x \text{ or } y \quad (40)$$

$W(\overline{r})$ is obtained from a convolution integral, so we have

$$\widetilde{W}(\overline{K}) = \widetilde{G}^F(\overline{K})\widetilde{S}(\overline{K}) \quad (41)$$

where $\widetilde{G}^F$ and $\widetilde{S}$ are the continuous Fourier transforms of G^F and S, respectively.

Analytical expressions for $\widetilde{G}^F$ can be found in the literature. For instance from [4] we have

$$\widetilde{G}^F(K_x, K_y) = \frac{(2\pi)^2}{T_x T_y} III\left(\overline{K}^{mn} - \overline{K}^i\right) \left[\frac{2\pi}{\left(K_x^2 + K_y^2 - K_o^2\right)^{1/2}}\right] \quad (42)$$

where

$$\overline{K}^{mn} = K_x^m \hat{x} + K_y^n \hat{y} = (2\pi m/T_x)\,\hat{x} + (2\pi n/T_y)\,\hat{y}$$

$$= m\left(T_x^K/N_x\right)\,\hat{x} + n\left(T_y^K/N_y\right)\,\hat{y}$$

$$\text{for} \qquad m, n = \pm 1, \pm 2, \ldots, \pm\infty \quad (43)$$

It can be noticed that $\widetilde{G}^F$ vanishes at all the spectral points except at $\overline{K} = \overline{K}^{mn} - \overline{K}^i$; so to compute $\widetilde{W}$ in (41) we only need to compute $\widetilde{S}$ for these points. It can be found that

$$\widetilde{S}\left(\overline{K}^{mn} - \overline{K}^i\right) = \widetilde{P}\left(\overline{K}^{mn}\right) \widetilde{S}^D(m, n) \quad (44)$$

where

$$\widetilde{P}\left(K_x, K_y\right) = \Delta x \Delta y \,\mathrm{sinc}\left(K_x \Delta x/2\right) \mathrm{sinc}\left(K_y \Delta y/2\right) \quad (45)$$

$$\widetilde{S}^D(m, n) = \sum_{i=0}^{N_x-1} \sum_{j=0}^{N_y-1} S^D(i, j) \exp\left(-j\left(K_x^m i \Delta x + K_y^n j \Delta y\right)\right)$$

$$= N_x N_y \,\mathrm{DFT}\left(S^D(i, j)\right) \quad (46)$$

The DFT indicates the Discrete Fourier Transform with a period of size (N_x, N_y)

A more useful expression for $\widetilde{W}(\overline{K})$ can be obtained by written the discrete variables (m,n) in (42)–(46) as follows

$$m = m_o + tN_x \tag{47a}$$
$$n = n_o + zN_y \tag{47b}$$

where m_o, n_o, t and z are integer variables and the first two of them must be:

$$0 \le m_o \le N_x - 1 \tag{48a}$$
$$0 \le n_o \le N_y - 1 \tag{48b}$$

Using the above variables $\widetilde{W}(\overline{K})$ can be expressed as follows:

$$\widetilde{W}(\overline{K}) = \sum_{m=-\infty}^{\infty} \sum_{n=-\infty}^{\infty} \delta\left(K_x - (K^m - K_{ox})\right) \delta\left(K_y - (K^n - K_{oy})\right) W^a\left(m/N_x, n/N_y\right) \widetilde{S}^D(m,n) \tag{49}$$

where

$$\begin{aligned} W^a\left(m/N_x, m/N_y\right) &= W^a\left(m_o/N_x + t, n_o/N_y + z\right) \\ &= \frac{(2\pi)^2 \Delta x \Delta y (-1)^t (-1)^z}{T_x T_y \pi^2 \left(m_o/N_x + t\right)\left(n_o/N_y + z\right)} \\ &\times \frac{2\pi \sin(\pi m_o/N_x) \sin(\pi n_o/N_y)}{\left(\left[(m_o/N_x + t)T_x^K - K_{ox}\right]^2 + \left[(n_o/N_y + z)T_y^K - K_{oy}\right]^2 - K_o^2 \right)^{1/2}} \end{aligned} \tag{50}$$

$$\widetilde{S}^D(m,n) = \widetilde{S}^D(m_o, n_o) \tag{51}$$

Relating (50), (51) and (38), we can write $W^\delta(\overline{K})$ in the following form

$$\widetilde{W}^\delta(\overline{K}) = \frac{1}{\Delta x \Delta y} \sum_{m'=-\infty}^{\infty} \sum_{n'=-\infty}^{\infty} \delta\left(K_x - (K^m - K_{ox})\right) \delta\left(K_y - (K^n - K_{oy})\right) W^p(m,n) \widetilde{S}^D(m,n) \tag{52}$$

where

$$W^p(m,n) = W^p(m_o + tN_x, n_o + zN_y) = W^p(m_o, n_o)$$
$$= \sum_{m'=-\infty}^{\infty} \sum_{n'=-\infty}^{\infty} W^a\left(m_o/N_x - m', n_o/N_y - n'\right) \quad (53)$$

As we could infer from the fact that $W^\delta(\bar{r})$ is obtained by sampling a periodic function in the real domain, $\widetilde{W}^\delta(\overline{K})$ is discrete and has a periodic nature, with a periodic cell of size (N_x, N_y) for the variables (m,n). So in this numerical approach we are dealing with functions that are discrete and periodic in both domains.

From (52) and (53) we can write $W^\delta(\bar{r})$ as

$$W^\delta(\bar{r}) = F^{-1}\left\{\widetilde{W}^\delta(\overline{K})\right\}$$
$$= \frac{1}{(2\pi)^2}\phi(\bar{r}) \sum_{m=0}^{N_x-1} \sum_{n=0}^{N_y-1} \delta(x - x^m)\,\delta(y - y^n)$$
$$\mathrm{DFT}^{-1}\left(W^p \widetilde{S}^D\right) \quad (54)$$

where DFT^{-1} indicates inverse discrete Fourier transform, with a period of size (N_x, N_y). It can be noticed that the convolution integral of part 3 of this paper can be computed efficiently by using only two FFT's, the direct FFT indicated in (46), and the inverse FFT of (54).

9.5 Computation of the Spectral Series

In this part the computation of the series of (53) is discussed. A first approximation to (53) is to consider only the first term $(m' = 0, n' = 0)$ in the series and to force W^p to be periodic

$$W^p(m,n) \approx W^a(m,n), \qquad \text{for} \begin{cases} 0 \le m \le N_x/2 \\ 0 \le n \le N_y/2 \end{cases} \quad (55a)$$
$$W^p(m,n) = W^p(m + tN_x,\, n + zN_y) \quad (55b)$$
$$W^p(m,n) = W^p(-m,-n) \quad (55c)$$

This approximation is considered in [1,3–5]. In [1] and [3] the convolution is made with the source function S expanded in terms of

rooftops instead of pulses as in (35) but only the corresponding first term of the spectral series is considered.

A second approximation to (53) is to consider the first $(2M)\times(2N)$ terms in the series

$$W^p(m,n) \approx \sum_{m'=-M}^{M-1} \sum_{n'=-N}^{N-1} W^a\left(m_o/N_x + m',\, n_o/N_y + n'\right) \qquad (56)$$

Examining the expression for W^a given in (50) it can be observed that in (53) the first four terms have the same sign and the other terms form a two-dimensional alternating series that decreases as

$$\frac{(-1)^{m'}(-1)^{n'}}{m'^2 n'^2} \qquad (57)$$

$W^p(m,n)$ can be computed accurately using an appropriate algorithm for this series. To do so, we have considered an algorithm due to van Wijngaarden, [14], and based on the Euler's transformation for alternating series.

Table 9.1 shows a comparison for $W^p(m,n)$, when this function is computed following (55), (56) with $M = N = 3$, and with the just mentioned algorithm, for the case $\Delta x = \Delta y = 0.1$, $N_x = N_y = 16$, $K_o = 2\pi$, $K_{ox} = K_{oy} = 0$. In this table the following values of (m,n) have been considered: $m = n = 0,1,2,\ldots,15$. It can be observed that for the values of (m,n) corresponding to the low spectral frequencies (for instance $m = n = 0,1,15$) the three approximations to W^p give nearly the same values. However for the central values of (m,n) (say $m = n = 7,8,9$) large differences appear between the computation of W^p using (55) and using van Wijngaarden's algorithm. However the differences between the computation using (56) and van Wijngaarden's algorithm are not significant. So it can be concluded that taking only one term for the series, as in (55), ripple problems can arise in the solution to the problem and these ripple problems can be made nearly negligible taking a few terms of the spectral series.

m - n	Using (55)	M - N - 3	Exact
0	.391E-2 + j.000	.391E-2 + j.000	.391E-2 + j.000
1	.825E-2 + j.000	.825E-2 - j.164E-4	.825E-2 - j.111E-4
2	.000 - j.254E-2	.000 - j.259E-2	.000 - j.258E-2
3	.000 - j.152E-2	.000 - j.141E-2	.000 - j.151E-2
4	.000 - j.993E-3	.000 - j.111E-2	.000 - j.109E-2
5	.000 - j.650E-3	.000 - j.914E-3	.000 - j.892E-3
6	.000 - j.461E-3	.000 - j.811E-3	.000 - j.786E-3
7	.000 - j.325E-3	.000 - j.762E-3	.000 - j.736E-3
8	.000 - j.226E-3	.000 - j.747E-3	.000 - j.721E-3
9	.000 - j.325E-3	.000 - j.762E-3	.000 - j.736E-3
10	.000 - j.461E-3	.000 - j.811E-3	.000 - j.786E-3
11	.000 - j.650E-3	.000 - j.914E-3	.000 - j.892E-3
12	.000 - j.993E-3	.000 - j.111E-2	.000 - j.109E-2
13	.000 - j.152E-2	.000 - j.141E-2	.000 - j.151E-2
14	.000 - j.254E-2	.000 - j.259E-2	.000 - j.258E-2
15	.825E-2 + j.000	.825E-2 - j.164E-4	.825E-2 - j.111E-4

Table 9.1 Comparison of results of computing W^p using three approximations.

9.6 Results

Three types of results are given:
– Current distributions on the square plate of a periodic lattice with a reference cell that is also square. A convergence study of the form of the current is included for different numbers of samples to represent the current and for different numbers of terms to compute the spectral series.
– A convergence study of the number of iterations required to obtain a fixed relative error for the periodic lattice considered in [15]. The relative error, ϵ, is defined as follows

$$\epsilon = \frac{\|LI - Y\|}{\|Y\|} \tag{58}$$

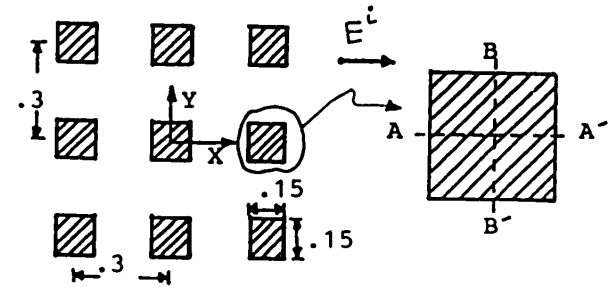

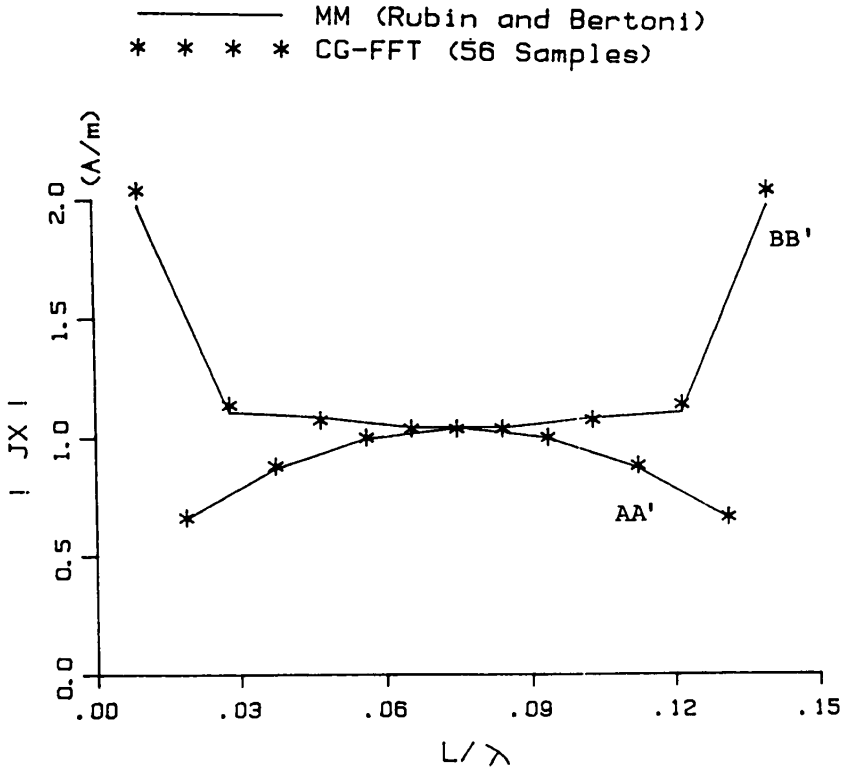

Figure 9.4 Amplitude of the co-polar surface current on a square plate of the lattice shown. All the dimensions of the lattice sketch are in wavelengths. The CG-FFT method is applied using $7 \times 8 = 56$ basis functions to represent each component of the current (J_x and J_y).

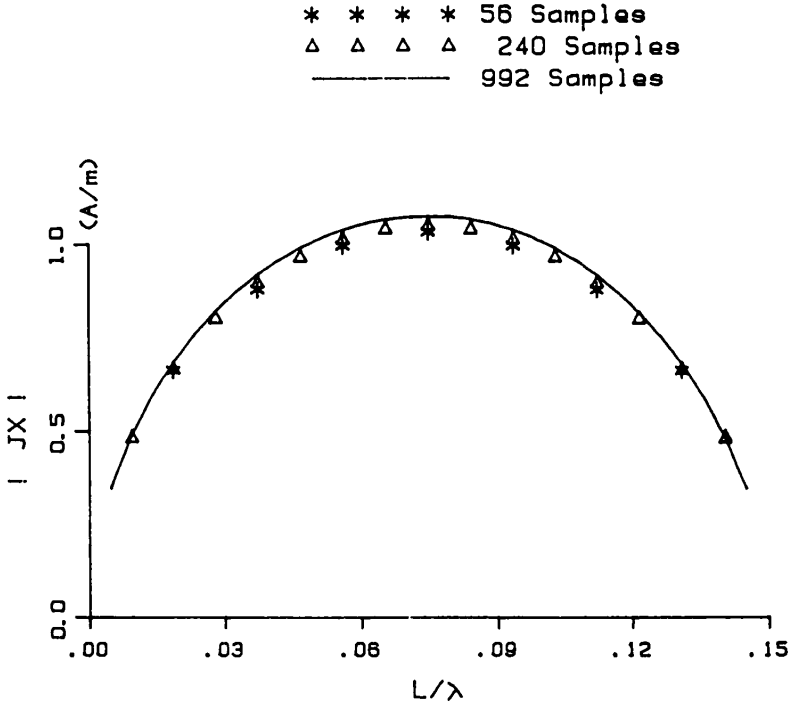

Figure 9.5 Results of a convergence study using CG-FFT method for the AA' cut in Fig. 9.4.

where $\|A\|$ indicates the norm of A.
– A comparison between reflection coefficient values resulting from our methods and measured or computed values taken from [16].

All the CG-FFT results for the current distributions and reflection or transmission coefficients were obtained with a relative error, less than 10^{-2} All results except those of Fig. 9.7 have been obtained using (56) with $M = N = 3$ for the computation of the spectral series.

A FPS-164 Array Processor with a VAX/750 has been used in all the computations presented here. The word length is 64 bits. The theoretical peak speed of this system is about 11 Mflops.

a. Current Distributions

Results for two current distribution cuts obtained using CG-FFT and MM, [2], are compared in Fig. 9.4. A plane wave is normally inci-

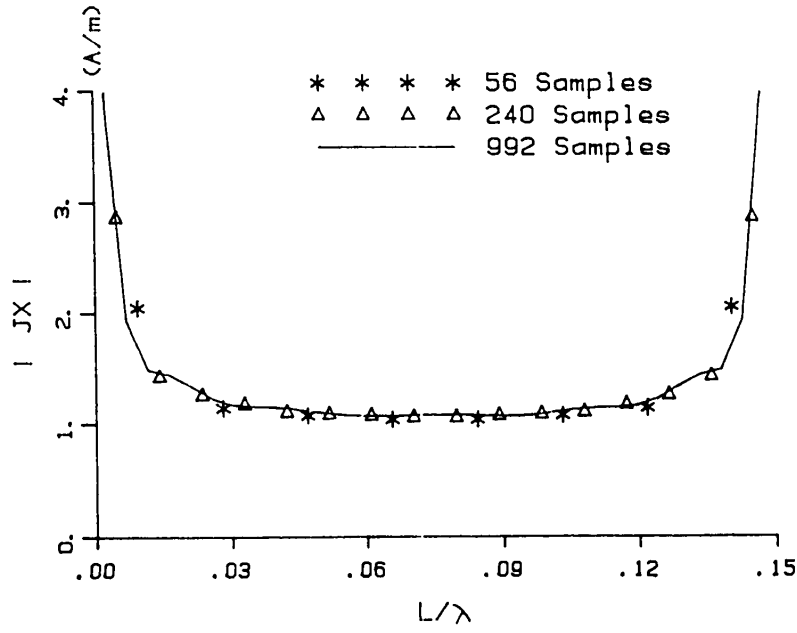

Figure 9.6 Results of a convergence study using CG-FFT method for the BB' cut in Fig. 9.4.

dent upon the periodic lattice shown in the figure. A similar number of basis functions was considered with both methods. The CG-FFT results were obtained by using (56) with $M = N = 3$. For the same situation Figs. 9.5–9.6 show a convergence study for the current distribution, using different numbers of rooftop functions but maintaining the number of terms considered to compute the spectral series, $(M = N = 3)$. It can be noticed that far from the plate edges the current for both cuts has a nearly stationary behavior when the number of rooftops is increased. As it is expected, near the edges the asymptotic behavior of the current is obtained better when the number of rooftops is increased. Fig. 9.7 shows the current distribution for the BB' cut considering three approximations in the spectral series computation. It can be noticed that the ripple in the curves is minimized when the number of terms in the series computation is increased.

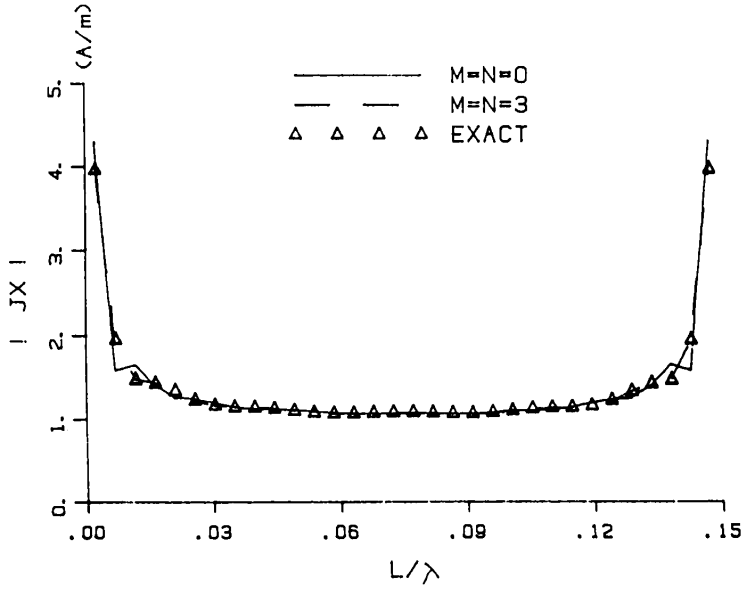

Figure 9.7 Comparison of current distributions for the BB' cut in Fig. 9.4 considering three approximations in the spectral series computation.

b. Convergence Study for the Number of Iterations

Figure 9.8 shows a comparison between the number of iterations required to obtain a relative error of .01 with our CG-FFT scheme and with those of [15], for the problem indicated in the figure. The best convergence rate is obtained with the present CG-FFT scheme that takes advantage of the efficient numerical technique developed in [8] to solve mixed-potential EFIE. Using this technique the Floquet's harmonic amplitudes for the induced current decays more fast.

Figure 9.9 shows curves of the evolution of the relative error versus the number of iterations for the problem indicated in Fig. 9.4. These curves show the typical behavior of the convergence evolution observed by author's in all their numerical experiments with this CG-FFT scheme. In short, it can be said that the number of iterations N_i required to obtain a fixed error is approximately proportional to

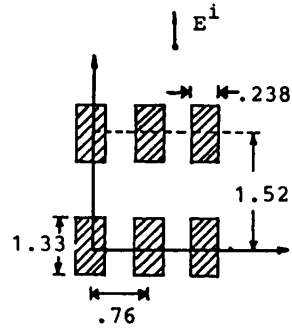

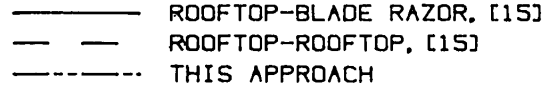

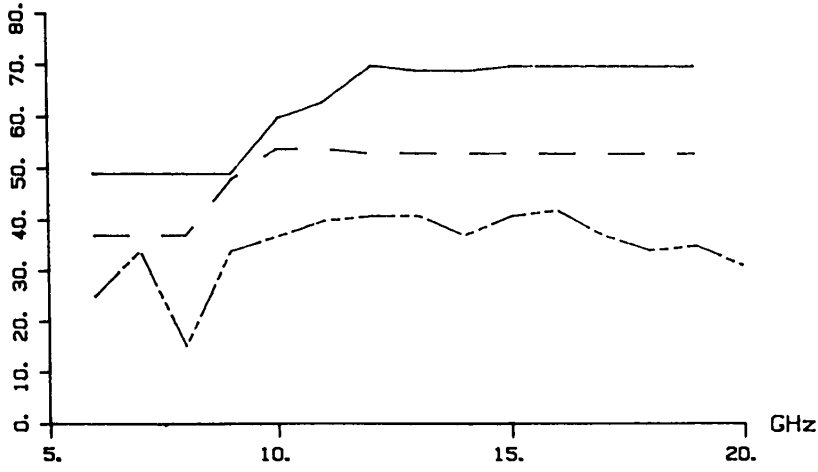

Figure 9.8 Comparison between the number of iterations required to obtain a relative error of 0.01 for the problem indicated. A grid with $N_x \times N_y = 16 \times 16$ is considered.

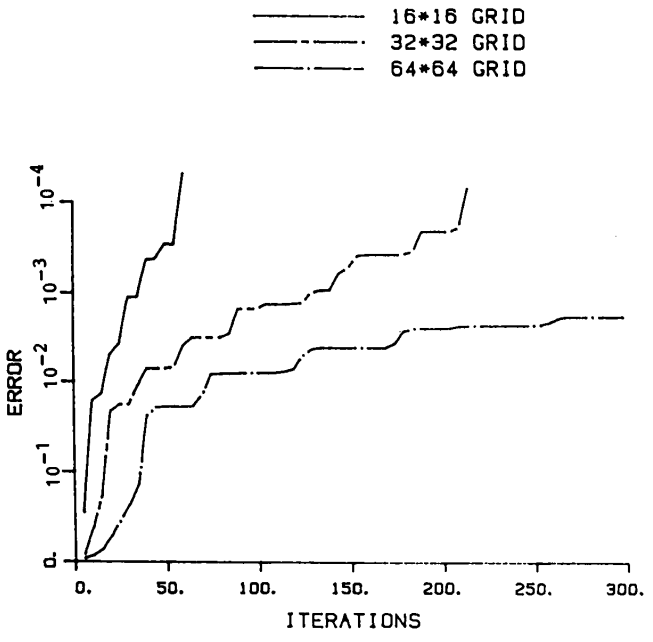

Figure 9.9 Results of a convergence study of the relative error for the problem indicated in Fig. 9.4 and considering three size for the discrete grid ($N_x \times N_y$).

$(N_xN_y)^{1/2}$. The computation time per iteration T_i is

$$T_i = AN_xN_y \log(N_xN_y)$$

So the total computation time to solve a problem with a given fixed relative error follows the law

$$t = A(N_xN_y)^{3/2} \log(N_xN_y)$$

The CPU time is about four minutes using the computer system previously indicated when $N_x = N_y = 64$. On the other hand, the memory requirements for the CG-FFT method is only several vectors of dimension N_xN_y. Therefore the CG-FFT scheme is efficient in computation time and memory requirements.

c. Reflection Coefficients

Figure 9.10 shows data for the reflection coefficient of the lattice indicated, at normal incidence, as a function of the frequency. The comparison is made with the computed and measured values that appear in [16]. It can be observed that the agreement between both computed values and the experimental results is good.

Figures 9.11–9.14 show the variations of the reflected TE and TM wave coefficients as a function of the angle of incidence , when a plane wave is incident with $\phi = 60°$ as indicated in Fig. 9.11. The CG-FFT results are compared with computed values by Chen, [16]. It can be observed in general a good agreement between both computed values for the magnitude of the TE and TM reflection coefficients. This is not the case for the phase of the reflection coefficients. Chen's phase values have a sharp change of nearly 180 for values of θ near 40°. This sharp change does not appear in the CG-FFT results. Authors are more confident on the CG-FFT results because those have been obtained considering nearly all the spectral band instead of a limited band as in [16].

9.7 Conclusions

A CG-FFT scheme to analyze FPS structures has been described. This scheme mainly presents two new features. First, the efficient scheme developed in [8,9] to solve mixed-potential EFIE is applied to FPS using the CG-FFT method. Second, the sampling of the fields in the real domain at equidistant points is explicitly recognized and used to avoid ripple problems that could appear otherwise. The results obtained show that this scheme is efficient and accurate for the purpose of designing FPS devices.

Appendix

Complete expressions to compute the scattered field and the inner products are given here.

The scattered fields E_x^{SD} and E_y^{SD}, (25)–(31), can be expressed

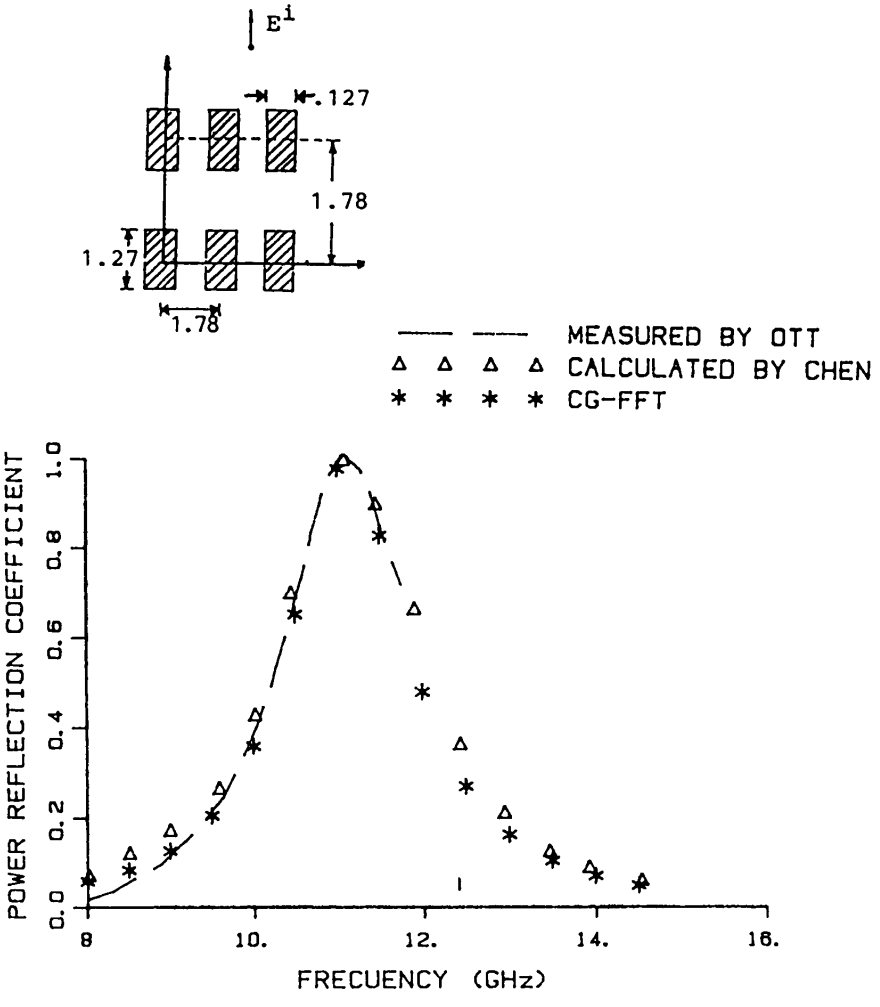

Figure 9.10 Comparison of results for the reflection coefficient of the problem indicated. The CG-FFT results were obtained using a grid-size with $N_x \times N_y = 32 \times 32$.

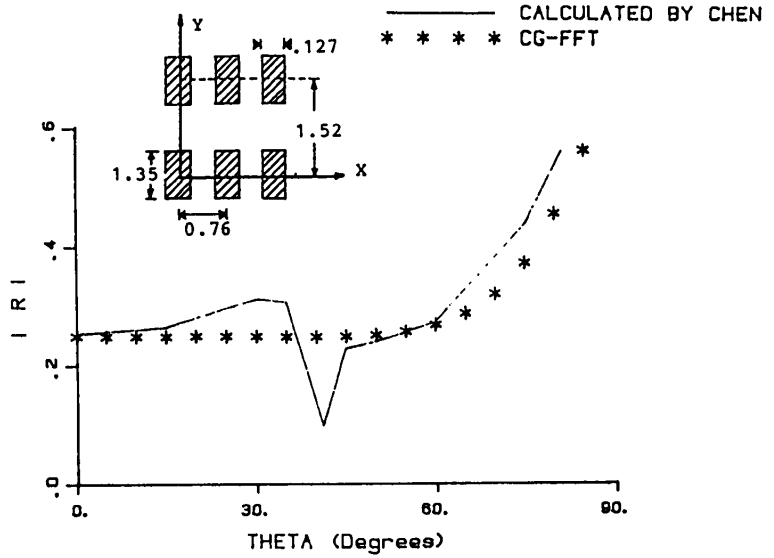

Figure 9.11 Comparison of results for the magnitude of the TE reflection coefficient as a function of the angle of incidence when a TE plane wave is incident upon the structure indicated with $\phi = 60°$. The CG-FFT results were obtained using a grid-size with $N_x \times N_y = 32 \times 32$.

as

$$E_\alpha^{SD} = \sum_{m=0}^{N_x-1} \sum_{n=0}^{N_y-1} \delta(x - x_\alpha^m)\,\delta(y - y_\alpha^n)\,E_\alpha^\delta(m,n) \qquad (A.1)$$

where $\alpha = x$ or y and E_α^δ is a discrete function that can be computed as follows

$$\begin{bmatrix} E_x^\delta \\ E_y^\delta \end{bmatrix} = F^{-1} \begin{bmatrix} C_x^I + C_x^Q\,(1 - F_x^*(i))\,(F_x(i) - 1) & C_x^Q\,(1 - F_x^*(i))\,(F_y(i) - 1) \\ C_y^Q\,(1 - F_y^*(j))\,(F_x(i) - 1) & C_y^I + C_y^Q\,(1 - F_y^*(j))\,(F_y(j) - 1) \end{bmatrix} \times \begin{bmatrix} W^p(i,j)F\left(J_x^D\right) \\ W^p(i,j)F\left(J_y^D\right) \end{bmatrix} \qquad (A.2)$$

$F(F^{-1})$ indicates direct (inverse) Fast Fourier Transform, and

$$C_\alpha^I = \left(\frac{N_x N_y}{(2\pi)^2}\right)\left(\frac{-j\mu\omega\Delta\alpha}{4\pi}\right) \qquad (A.3)$$

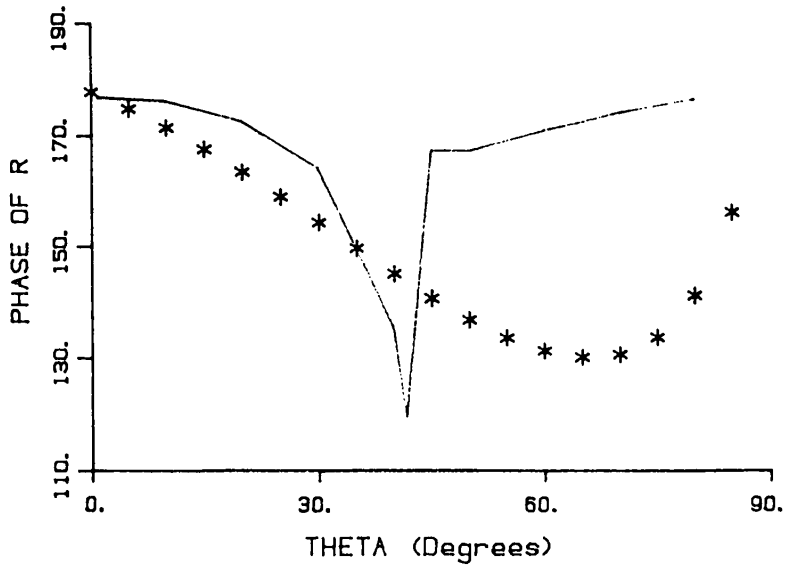

Figure 9.12 Phase results, for the reflection coefficient, case TE-TE, for the problem indicated in Fig. 9.11.

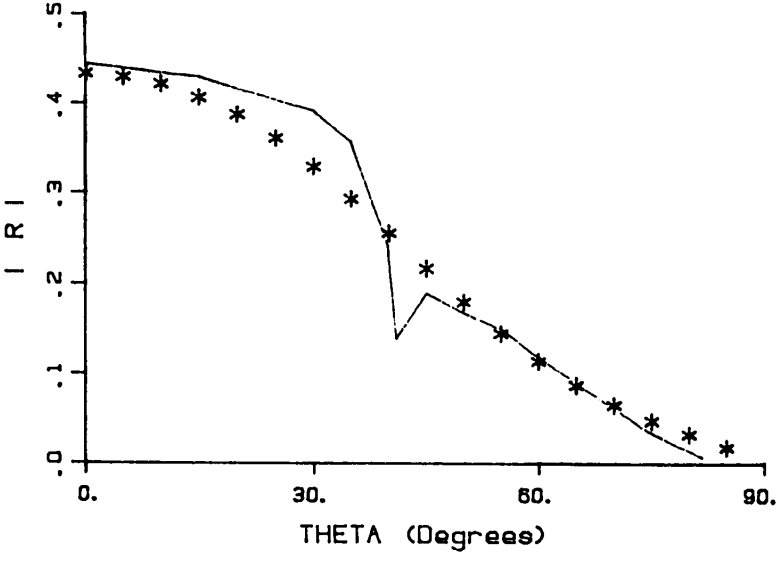

Figure 9.13 Magnitude results for the reflection coefficient, case TE-TM, for the problem indicated in Fig. 9.11.

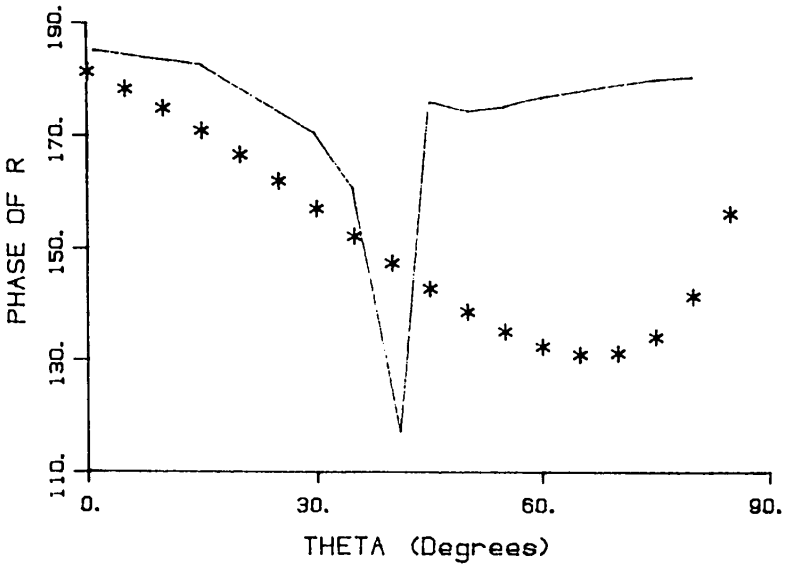

Figure 9.14 Phase results for the reflection coefficient, case TE-TM, for the problem indicated in Fig. 9.11.

$$C_\alpha^Q = \left(\frac{N_x N_y}{(2\pi)^2}\right)\left(\frac{-j}{4\pi\epsilon\omega\Delta\alpha}\right) \tag{A.4}$$

$$F_\alpha(i) = \exp(j2\pi i/N_\alpha) - jK_{o\alpha}\Delta\alpha \tag{A.5}$$

F_α^* is the complex conjugate of F_α

W^p is given in (53) and J_x^D, J_y^D are given in (17).

The inner product computations required in the CGM algorithm can be evaluated as follows

$$\left\langle J^a, E(J^b)\right\rangle = \left\langle J_x^a, E_x(J^b)\right\rangle + \left\langle J_y^a, E_y(J^b)\right\rangle = \left\langle J_x^a, E_x^b\right\rangle + \left\langle J_y^a, E_y^b\right\rangle \tag{A.6}$$

where the scalar inner product of J_α^a and E_α^b is

$$\langle J_\alpha^a, E_\alpha^b\rangle = \int_{S_p} J_\alpha^a \left(E_\alpha^b\right)^* ds$$

$$= \int \left(\sum_{i=0}^{N_x-1} \sum_{j=0}^{N_y-1} J_\alpha^{aD}(i,j)\, T_\alpha^{ij}(\bar{r}) \right)$$
$$\times \sum_{i'=0}^{N_x-1} \sum_{j'=0}^{N_y-1} \delta\left(x - x^{i'}{}_\alpha\right) \delta\left(y - y^{j'}{}_\alpha\right) E_\alpha^{b\delta^*}(i',j')ds$$
$$= \sum_{i=0}^{N_x-1} \sum_{j=0}^{N_y-1} J_\alpha^{aD}(i,j)\, E_\alpha^{b\delta^*}(i,j) \qquad (A.7)$$

J_α^{aD} and $E_\alpha^{b\delta}$ are obtained by expanding J_α^a and E_α^b as shown in (17) and in $(A.1)$, respectively.

Finally the discrete adjoint operator is given by

$$\begin{bmatrix} E_x^{\delta,adj} \\ E_y^{\delta,adj} \end{bmatrix} = F^{-1} \begin{bmatrix} C_x^{I^*} + C_x^{Q^*}(1 - F_x(i))(F_x^*(i) - 1) & C_x^{Q^*}(1 - F_x(i))(F_y^*(j) - 1) \\ C_y^{Q^*}(1 - F_y(j))(F_x^*(i) - 1) & C_y^{I^*} + C_y^{Q^*}(1 - F_y(j))(F_y^*(j) - 1) \end{bmatrix} \times \begin{bmatrix} W^{p^*}(i,j) F(J_x^D) \\ W^{p^*}(i,j) F(J_y^D) \end{bmatrix} \qquad (A.8)$$

where $E_\alpha^{\delta,adj}$ means the adjoint of E_α^δ.

Acknowledgments

This work has been supported by the Spanish Advisory Commission for Scientific and Technological Research (CAICYT), Project No. PA 86-0395.

References

[1] Cwik, T., and R. Mittra, "Scattering from general periodic screens," *Electromagnetics*, **5**, 263–283, 1985.

[2] Rubin, B. J., and H. L. Bertoni, "Reflection from a periodically perforated plane using a subsectional current approximation," *IEEE Trans. Antennas Propagat.*, **AP-31**, 829–836, 1983.

[3] Cwik, T. A., and R. Mittra, "Scattering from a periodic array of free-standing arbitrarily shaped perfectly conducting or resistive patches," *IEEE Trans. Antennas Propagat.*, **AP-35**, 1226–1234, 1987.

[4] Cátedra, M. F., R. P. Torres, and J. G. Cuevas, "A method to analyze scattering from general periodic screens using Fast Fourier Transform and Conjugate Gradient Method," Presented at NATO Advanced Study Institute on Electromagnetic Modeling and Measurements for Analysis and for Synthesis Problems, Il Ciocco, Italy, August, 1987 (to appear in proceedings published by Sijthoff & Noordhoff, The Netherlands).

[5] Cátedra, M. F., and R. P. Torres, "A new Conjugate Gradient – Fast Fourier Transform (CG-FFT) scheme for analysis and design of flat metallic periodic structures," *IEEE AP-S International Symposium,* Syracuse, NY., 99–102, 1988.

[6] Sarkar, T. K., and S. M. Rao, "The application of the Conjugate Gradient Method for the solution of electromagnetic scattering from arbitrarily oriented wire antennas," *IEEE Trans. Antennas Propagat.*, **AP-32**, 398–403, 1984.

[7] Peterson, A. F., "An analysis of the spectral iterative technique for electromagnetic scattering from individual and periodic structures," *Electromagnetics,* **6**, 255–276, 1986.

[8] Glisson, A. W., and D. R. Wilton, "Simple and efficient numerical methods for problems of electromagnetic radiation and scattering from surfaces," *IEEE Trans. Antennas Propagat.*, **AP-28**, 593–603, 1980.

[9] Pearson, L. W., "A technique for organizing large moment calculations for use with iterative solutions method," *IEEE Trans. Antennas Propagat.*, **AP-33**, 1031–1033, 1985.

[10] Popovic, B. D., M. B. Dragovic, and A. R. Djordjevic, *Analysis and Synthesis of Wire Antennas,* Chichester: Research Studies Press, 1982.

[11] Elliot, D. F., and K. R. Rao, *Fast Transforms, Algorithms, Analysis Applications,* Academic Press, 1982.

[12] Bracewell, R. N., *The Fourier Transform and Its Applications,* Second edition, McGraw-Hill, 1978.

[13] Cátedra, M. F., J. G. Cuevas, and L. Nuño, "A scheme to analyze conductor plates of resonant size using the Conjugate-Gradient Method and the Fast Fourier Transform," *IEEE Trans. Antennas Propagat.*, **AP-36**, No. 12, 1744–1752, December 1988.

[14] Press, W. H., B. P. Flannery, S. A. Teakolsky, and W. T. Vetterling, *Numerical Recipes, The Art of Scientific Computing*, Cambridge University Press, Cambridge 1986.

[15] Chan, C. H., and R. Mittra, "Convergence studies of conjugate gradient method applied to frequency selective surface problems using subdomain basis functions," *1987 IEEE AP-S International Symposium Digest*, 87–89, Blacksburg 1987.

[16] Chen, C. C., "Scattering by a two dimensional periodic array of conducting plates," *IEEE Trans. Antennas Propagat.*, **AP-18**, 660–665, September 1970.